Image analysis on the structure of the Achilles Tendon

Linnea Andersson

Lund, January 2022

LUND
UNIVERSITY

Master's Thesis in
Biomedical Engineering

Faculty of Engineering, LTH
Department of Biomedical Engineering

Supervisors: Maria Pierantoni & Hanna Isaksson

Title
Image analysis on the structure of the Achilles tendon

Author
Linnea Andersson

Figures
Created by the author if nothing else is indicated

Lunds Universitet
Institutionen för biomedicinsk teknik
Box 118
SE-221 00 Lund
Sverige

E-husets tryckeri
Lund 2021

Acknowledgements

First I would like to thank my supervisors, Maria Pierantoni and Hanna Isaksson and my examiner Anna Gustafsson, without you this project would not be finished. I would also like to thank the Biomechanics group at LTH for the nice company they have provided during meetings and common outings. A special thanks to the PhD students and other Master thesis students that have presented their works during my time in the group, your works have been very inspiring to listen to and take part in! I would also like to thank my family for all their support which they have provided in many different ways. Lastly I would like to say a big thanks to my friends and classmates who really have made these interesting times bearable by keeping me company and helping me by exchanging ideas, providing experienced tips and help at all times. A special thanks to my roommate Leo, who has been especially helpful and I appreciate dearly.

Abstract

The Achilles tendon is the largest tendon of the human body which makes injuries of it very painful and incapacitating. A common factor of the pain are heterotopic ossifications, which are mineral deposits occurring inside the normal tendon tissue. Why and how heterotopic ossifications occur are somewhat unknown. To investigate this, many different methods of study have been trialed by scientists to create a complete understanding of the underlying causes. As new scientific methods and principles are developed, the understanding of our inner structures are increased.

In this project, image analysis methodologies have been applied to high resolution images taken of rat Achilles tendons. The rats either had an forced unloading of their right leg, had their tendon microinjured by needling or was part of a control group. These animal experiments and image production was not done as part of this thesis but of a larger Achilles tendon project. The animal experiments were performed by Dr. Malin Hammerman and the imaging was done by Dr. Maria Pierantoni.

This thesis has focused on producing a segmentation of the whole tendon as well as the hetrotopic ossification minerals. Different image analysis methods have been tried to achieve this, including different filters and morphological operations. Different pipelines had to be developed for extracting the soft tendon tissue and the hard mineral since they intrinsically look different on an x-ray image. The segmented mineral and tendons were then compared in relation to their testing group. To compare them different metrics were extracted; the volume and placement of the mineral as well as the volume of the tendon.

No substantial differences were found between any of the groups, but tendencies in mineral volume and placement could distinguish the groups.

With regards to the segmentation, there are specific places within the data sets that segments well and others that segment worse.

This study does not answer the question on why hetrotopic ossifications occur, although the observations are not conclusive, there are still some points that can indicate a relationship connecting loading and microinjuries to heterotopic ossification of the tendon. This was observed as the variance, in the groups that were not part of the control, had generally less variation within their groups in many of the trialed metrics. Hetrotopic ossifications were evidently present in all but one of the trialed tendons, hence it is surely a common part of the natural tendon.

Contents

Chapter 1

Introduction

Biomechanics is a broad subject which goal is to understand how forces and pressures are translated through biological tissues and organisms. Focus is to understand the relation between movement of the muscoskeletal system and mechanical forces within tissues and structures. Both forces on the body and forces that are produced inside the system are of interest to understand damage of our tissues and how they work regularly. One of the more complicated tissues in our body is the tendon due to its time dependent elasticity response to forces. While significant effort has been put in studying tendons, new x-ray imaging techniques using particle accelerators gives us new insights into the microscopic inner structure that was previously, at least partly, unknown.

The muscoskeletal tissues in our body can be divided into two groups, hard and soft tissues. Tendons are a soft tissue along with, among others, muscles. In comparison to hard tissues they are more flexible and often act as connectors and protecting layers for other tissues. Bones are in general more hard and less flexible.

To study how our bodies respond to different loading scenarios in everyday life, scientist often look to the more controlled environment of animal testing. When studying differences in biological response in tendons common practice is to use distinct loading protocols to, for example, identify differences between a tendon which has endured a more active lifestyle compared to one which has been more sedentary [1]. Testing usually consist of a control group and one or more testing groups which has gone through different loading regimes and or other changes that can affect movement or biological responses [2]. Testing how incapabil-

ity to move the leg affects the shape and structure of the tendon can be simulated in an animal model by letting a test group of animals wear a boot on one leg (so to partially being unable to move it) and letting a control group move normally [2].

Pain and inability to move the tendon can occur due to so called microinjuries, micrometrical tissue damages. These appear as a prelude to total mechanical material rupture and also to further tendon injuries and ailments [3]. One of these are heterotopic ossification, which is a process where bonelike mineral fragments are formed within the tissue, disabling normal mechanical response [4]. Why and how these appear is still unknown. Experimental methods using tensile force are used in a wide sense to understand the mechanical response but can't directly say anything on the inner structure, so using only these methods will not be able to tell us anything about the mineral formation process. Histological experiments that use tissue staining can, on the other hand, reveal what substances are active inside the tissue [5]. The limitations of this method is that it is a 2D microscopy technique, this means destruction of the sample is necessary to extract data. This makes it an inefficient method to obtain a complete 3D representation of the tested tissue.

Animal testing with different loading regimes or modifications to tissue in combination with modern x-ray tomographic imaging can help understand the extent of the ossification. Techniques using synchrotron light sources, such as MAX IV in Lund, can with x-rays produce high quality images in short amounts of time. This can be the key to unlocking more information in relation to tissue structure and healing. In combination with animal testing using different loading regimes the origin of mineral tissue and microinjuries has a possibility of being determined. Because the imaging process is fast, 3D reconstruction of the sample is possible from the images. This opens up an alternative to observing samples without cutting them and risking destroying parts of the structure [6]. Modern image processing and analysis techniques can be essential for completing the understanding of the most inner structure of our bodies such as the building blocks of the tendon.

1.1 Aim

This project aims to investigate two data sets, one where different loading scenarios have been applied to the specimens and one where the specimens have had their tendons microinjured with needles to different degrees. Based on image data collected using high resolution phase contrast enhanced tomography from these two experiments, this thesis aims to develop an image analysis pipeline to quantify the ossification of the tendons. With this information inquries will be made to better understand the the inner structural changes of the tendon. The objective is to answer the following questions:

- To what extent does ossification occur in the rat Achilles tendon?
- If ossification occur, does the extent differ
  a) between rats where the tendons were normally loaded compared to those that were unloaded (by a botox injection in combination with a boot) and
  b) between control rats and those where microinjuries were performed (by needling)?

1.2 Design of the study

The starting point of this thesis was sets of 3D synchrotron x-ray images of rat tendons that had previously been part of a larger study. There were seven samples each from the groups of the first study, which examined different loading scenarios, and three samples for each of the groups of the second study, which examined different amounts of microinjuries. The images have been taken at a synchrotron radiation facility and are of micrometrical resolution. To analyse the change in volume of the tendon and also localize ossification in the tendon computer based image analysis has been used (figure 1.1).

This project has not been looking deeper into what causes heterotopic ossification but rather just looked at the specific connection to loading and microinjuries within the tendon. The data used in this thesis was collected and produced before the thesis began. More raw data will not be collected in or for thesis project.

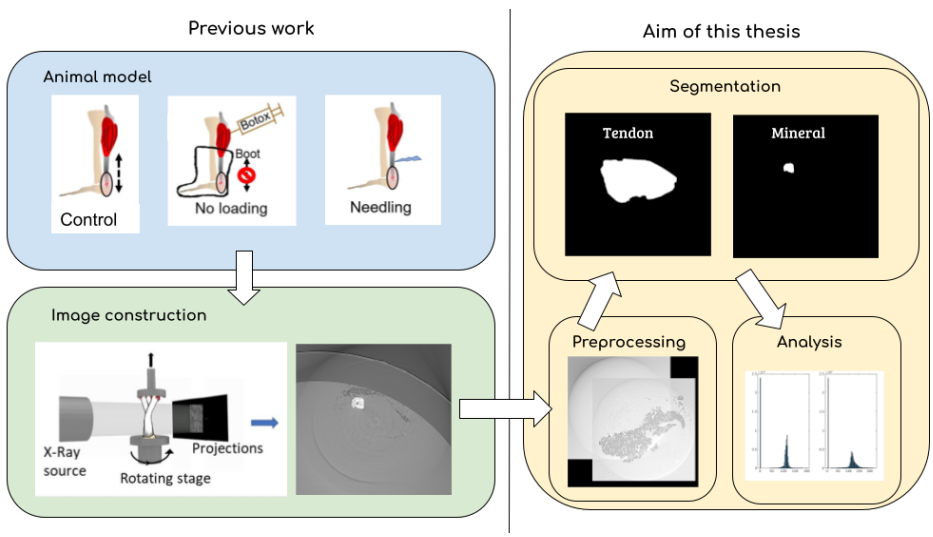

Figure 1.1: A graphic representation of this thesis work.

Chapter 2

Theory

2.1 The Achilles tendon

The Achilles tendon is the thickest tendon in the human body. However, it is also the most common tendon to rupture [7]. This makes it a very interesting subject for analysing in relation to different loading regimes and its structure pre, intra and post injury and healing. The main function of tendons is to translate forces between muscles and bones, which enables movement. It has been shown that the structure of the tendon is highly correlated with the function it has and how much stresses and strains it is subjected to [8]. This is why the Achilles tendon is so thick, it translates the entire stress of the body weight in each step the body takes. During running, forces that travel through the Achilles tendon measures to about two or three times the body weight of the person [9]. One of the highest measurements of the force transmitted through the Achilles tendon peaked at $9kN$ which was 12.5 times the body weight of the subject [1].

2.1.1 Animal models for human Achilles tendon

Experiments on human tissues are not very common, both because of the ethical implications and because it is difficult to achieve controlled and standardised loading scenarios. It is therefore common to use rats as a model when studying different research questions related to the Achilles tendon. Rats have been used for experiments for a long time historically so their physiology is very well understood. Their small size and fast growth rate also promotes the use of them compared to other

animals.

2.2 Anatomy

The Achilles tendon is located at the posterior side of the leg. It links between the heel bone, also known as the calcaneal bone, and the calf muscles in the lower leg (figure 2.1). Rat anatomy is similar to human Achilles tendon anatomy, although there are differences mainly due to the differences in size of the two species [10]. In an article by Lee and Elliott [10] it was shown that the rat tendon is not just a scaled down version of human or other larger animals. The thickness for the collagen fiber in rats was shown by this study to be between 10 and $50\mu m$, it has previously been shown that human collagen fibers are around $15\mu m$ and equine collagen fibers range between 1 and $20\mu m$ [10]. This is a very similar range and Lee and Elliott therefore come to their conclusion that rat Achilles tendon does not have the same hierarchical structure as larger animals, since the fascicle layer is not present. The study also showed significant difference in the plantaris tendon, which is a smaller tendon in the same area as the Achilles tendon, connected to the plantaris muscle. The plantaris tendon has the same insertion site in all rats while its insertion varies in humans which led scientists to believe it was not present in most humans [10]. Figure 2.1 shows the full tendons insertion into the calcaneal bone and the separation of the tendon into three subtendons. These subtendons connect to one each of the three muscles (soleus, lateral gastrocnemius and medial gastrocnemius) of the posterior leg in a rat tendon. The same structure of the tendon can be observed in humans.

2.2.1 Composition

Like all body tissues tendons have a specific material content which consists of cells, collagens, glycoproteins, proteoglycans and water. Out of the dry mass in a tendon about 60% is collagen, primarily collagen type I, with trace amounts of type III and type V which can often be found at specific parts of the tendon [1]. Collagen I is an oblong shaped molecule which first was thought to be quite unflexible but it was later discovered that has some bending points along its triple helix structure [11]. As previously mentioned the tendon structure is built on the different layers of collagen organization. This structure is an example of

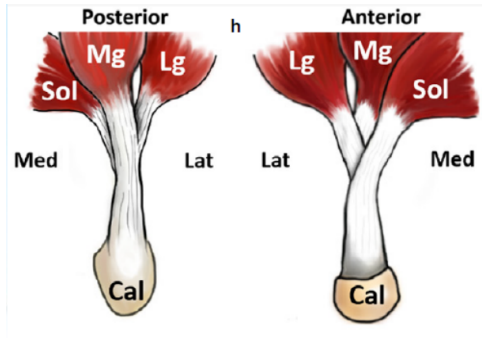

Figure 2.1: Illustration of a rat Achilles tendon from Lee et al. [10]. Sol = Soleus muscle, Lg = Lateral gastrocnemius and Mg = Medial gastrocnemius.

collagen self-assembly which means that the collagen naturally assumes this type of structure in the tendon [11].

One of the interesting less common components of the tendon structure is the proteoglycans, which is a group of molecules more common in cartilage. Mainly, the function of proteoglycans is to increase the resistance to compressional forces. This is done by increasing (or decreasing) the swelling pressure and hydration within the tissue [12]. The amount of proteoglycans varies a lot w.r.t. the function of the tendon or tendon part in particular. In some bovine tendons, which are mainly compressed under normal use, the proteoglycan content is high (3.5% of the dry weight in this case) but in their tensile stretching tendons it is low (only $0.2-0.5\%$) [1]. How the different collagens, proteoglycans etc. are arranged in the tendon has an immediate effect on the mechanical behaviour [11].

2.2.2 Structure and biology

It has been shown that the structure of the tendon is highly correlated with the function it has, and how much stresses and strains it is subjected to [8]. The inner structure of a tendon contains many different layers (figures 2.2 and 2.3). The base of this structure hierarchy is the collagen molecule. Collagen then organizes itself into bunches called fibrils and these bunch up into fibers. Some studies indicate that be-

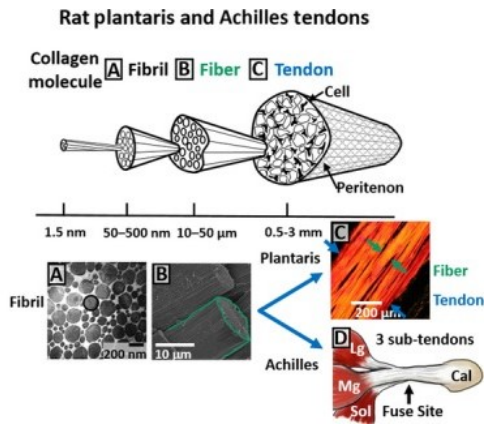

Figure 2.2: The inner structure of a rat Achilles tendon, taken from *Comparative multi-scale hierarchical structure of the tail, plantaris, and Achilles tendons in the rat* by Andrea H. Lee and Dawn M. Elliott [10].

cause of the small size of the rat, these fibers is what the whole tendon consists of while human and other larger animals require a further layer of fascicles, which then combines into the tendon [10]. This has not reached a consensus in the scientific community though, rats may also have the further layers of inner structure in their tendon. Each of the described structural levels can also be divided into more sublevels (subfascicle etc), which have the same main functions as their progenitor [14]. To achieve the desired mechanical function and longevity all of these levels run in the main direction of the tendon [11]. In the Achilles tendon we also make the distinction between fascicles and the so called subtendon which connects the tendon to each muscle respectively [15]. These subtendons are usually of similar size as fascicles but distinguishes from fascicles by connecting to a specific muscle (figure 2.1).

2.2.3 The mechanical response of the tendon

In addition to all these different layers, tendon fibrils and fibers are known to have a particular structural feature called crimp. The crimp is the result of a very distinctive arrangement of the fibrils folding themselves when the tendon is relaxed. When tension is put on the tendon the crimp is straightened out [8]. This affects the strain response from stress of the tendon, this corresponds to the toe region of the stress-strain curve (figure 2.4) [1]. This crimping pattern varies in angle and length depending on what tendon it is, which is a response of the par-

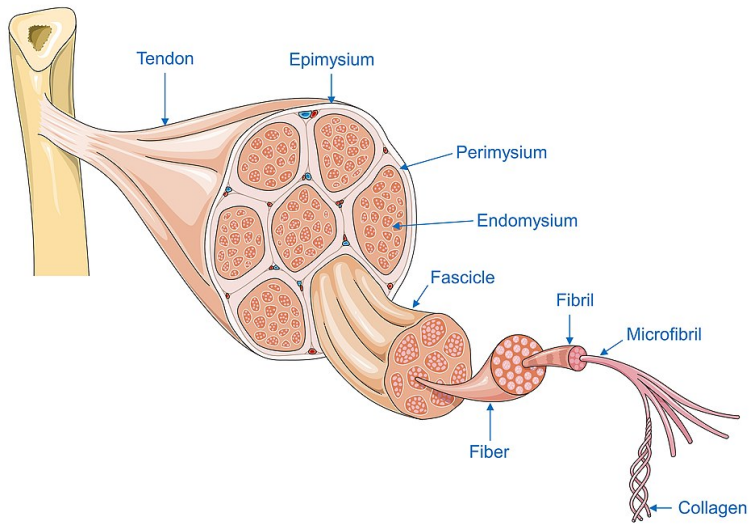

Figure 2.3: The inner structure of the human tendon [13].

ticular mechanical function of the tendon. Tendons with lesser crimp angles will experience microscopic failure in response to smaller applied forces. After the crimp is stretched out the tendon will in general behave in a linear way, as displayed in figure 2.4 [1].

A way to model the entire loading response of the tendon mechanical behaviour is using viscoelastic models. These are models that combine dampening elements (viscous behaviour) and elastic elements (elastic behaviour). In a model, these are represented by a dashpot or a spring respectively. At lower strain rates, the tendon is easily reshaped and absorb the energy of the weight which is not very effective in moving large loads. When the strain is higher and the crimps stretches out the tendon becomes more stiff and can transfer larger loads[1]. Other than the crimp, collagen fibril and fiber sliding inside collagen rich biological tissues also exists [16]. This has a significant effect on the elongation of the tendon which will change the absorption of forces and have effect on the final mechanical behaviour. In figure 2.4 there is also a point of microscopic failure that occurs before the total rupture of the tissue occurs. Microscopic failure here means that the inner structure in the tendon fails in some way e.g. breaking of the collagen fibrils. This also has an effect on the mechanical behaviour before the rupture happens.

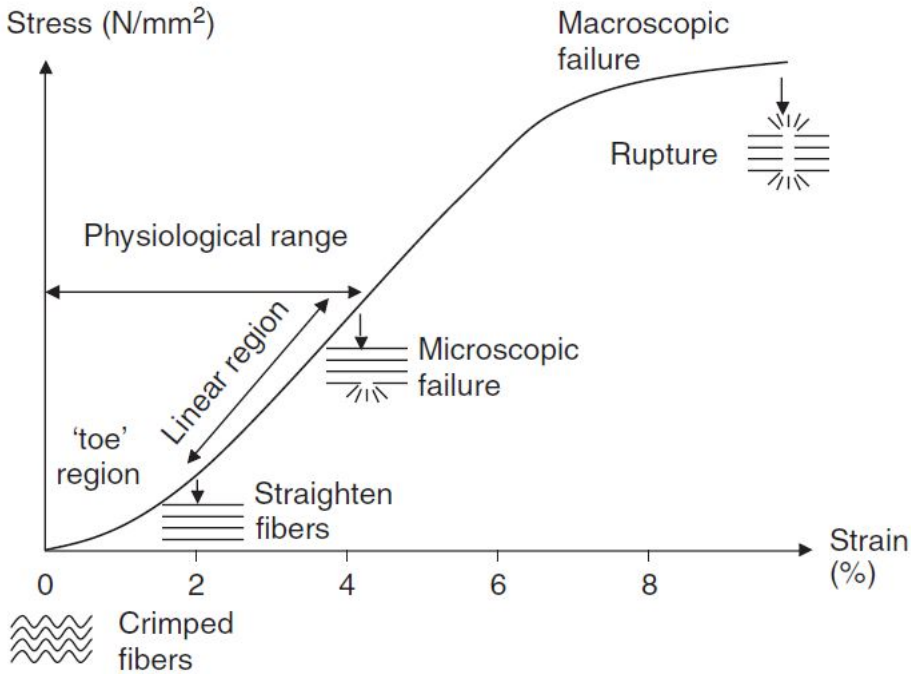

Figure 2.4: A general stress strain curve for tendons [1].

2.3 Heterotopic ossification

Among the many pathologies that can affect a tendon, calcific tendonitis is common in the Achilles tendon and consists of the formation of calcific deposits inside the tendon soft tissue. These deposits are also called heterotopic ossifications and can occur due to traumatic incidences of the soft tissue but can also be a genetic complication although the non-genetic is more prevalent [4]. This leads to pain and reduced function of the tendon. In some animals this calcification occurs naturally as a part of their developing or ageing body, for example in young turkey Achilles tendons, it is due to the skeletal changes of the turkey body [11]. The calcifications can also be stimulated by both overloading and rupture of the tendon [3]. Lin et al. found a significant difference in heterotopic ossification of the contralateral (left) tendon of mice who had received a full Achilles tenotomy on their right tendon compared to a control group. The left tendon had micro tears and also ossifications were present at both ends of the tendon [3]. The calcifications were

hypothesised to have appeared because of an surplus of metabolically active cells which promoted the ossification.

Mineral deposits can have an effect on the biomechanical properties of the tendon [3]. As a result of this the tendon becomes more stiff [11]. These minerals may also hinder the crimp to stretch, molecular deformation and sliding of the tendon, which in turn affect all layers larger than molecular level. Due to tendinopathy also the cross sectional area was decreased slightly in the study by Lin et al., as well as the maximal failure load was noteably reduced and the stiffness was significantly increased [3].

2.4 Micro CT imaging

Historically the main method used to identify the composition and structure of tissues has been histological staining using chemicals that activate certain substances and materials within the tissue [5]. These methods are mostly two dimensional which means the sample has to be sectioned [5]. The 3D rendering of this also has the problem of artefacts at all cutting edges and is also very labor intensive [5]. Even electron microscopes can not create a cohesive 3D image, as the penetration depth is too short which causes that the sample should be cut into multiple pieces [17].

Radiography is a technique mainly used for 2D imaging in many hospitals for diagnostic purposes, X-ray imaging is also the base of the 3D imaging convention Computed Tomography (more commonly known as CT). CT is a noninvasive way to look at the internal structure of tissues and is especially useful to identify bone in relation to soft tissues [18]. To understand tissues on a micrometrical scale μCT is used by scientists. This is a higher resolution X-ray that offers higher resolutions of the output compared to regular CT which makes it highly suitable for obtaining experimental data of small animals [18].

X-ray tomography is a good method for high resolution imaging, however, a limitation that cannot be overcome by just looking at the microscopic scale is the tissue contrast. Soft tissues often hold much water and appear to have similar and low contrast when imaged through an X-ray. To better understand the microstructure of especially weakly absorbing

tissues, as for instance the tendon soft tissue, scientists have developed 3D imaging techniques using both synchrotron light sources and smaller benchtop x-ray machines [6], [17]. By introducing phase contrast microscopy the contrast of these tissues are greatly enhanced and can more accurately be differentiated [19]. This is done by placing the specimens at specific distances from the outgoing beam, as illustrated in figure 2.5.

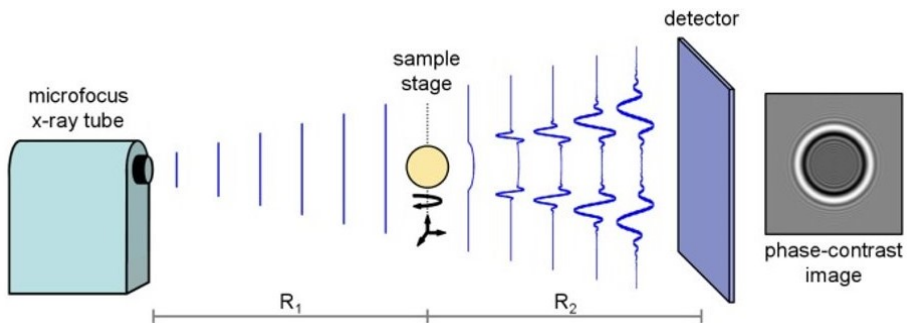

Figure 2.5: Imaging setup illustrating the concept of phase contrast tomography, in this case of an eye [17].

By using coherent light sources (such as a synchrotron) exploitation of the synchronized wave propagation is made possible. This enables the usage of phase shift which can increase the contrast of tissues that have a low absorption of the light [20]. Sub-micrometric images can be taken at quicker speeds and in a readily way using synchrotron light ray sources [6]. These are also easy to reconstruct back into 3D using regridding algorithms.

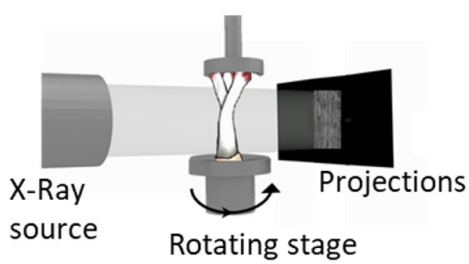

Figure 2.6: An illustration of the setup for producing high resolution images from a synchrotron [6].

2.5 Image processing

Image processing consists of different techniques for which an image or image set is treated to extract new information. Some methodologies have been listed as *Preprocessing* steps because, they have in this report been used as steps to enable the later analysis.

2.5.1 Preprocessing

Conversion from 16bit to 8bit and downscaling

To reduce the processing time and also reducing the computational costs the data needed to be downsized. Decreasing image size has two clearer easy methods, lessen the number of pixels and reducing the amount of greylevels.

Most commonly the number of greylevels in a greyscale image is a power of two, most commonly 2^8, 2^{16} or 2^{32} also called 8bit, 16bit and 32bit images respectively, where the greylevels go from 0 to $2^n - 1$. An example of reducing greylevels can be seen in table 2.1. In order to downsize the greyscale from $n$bit to $n/2$bit, different methods can be used for deciding what the appropriate downsizing conversion is. One way to proceed would be to adapt a regular normalizing formula, seen in eq. 2.1.

$$X_{normalized} = \frac{X - x_{min}}{x_{max} - x_{min}}. \tag{2.1}$$

From this, one obtains numbers ranging from 0 to 1 which can be adjusted to the new $n/2$bit by multiplying with its largest value and rounding so that it is an integer value. For greyscale the levels start at 0 which gives the variables $x_{max} = 2^n - 1$ and $x_{min} = 0$, which simplifies the formula (eq. 2.2)

$$Im_{n/2} = round((2^{n/2} - 1) * \frac{Im_n - 0}{2^n - 1 - 0}) = round(Im_n * \frac{2^{n/2} - 1}{2^n - 1}) \tag{2.2}$$

In this thesis specifically conversion between 8bit and 16bit have been used, an example of this can be seen in equation 2.3:

$$round\left(\begin{bmatrix} 65535 & 999 & 27 \\ 17889 & 35004 & 20573 \\ 55851 & 29200 & 8186 \end{bmatrix} * \frac{2^8 - 1}{2^{16} - 1}\right) = \begin{bmatrix} 255 & 4 & 0 \\ 70 & 136 & 80 \\ 217 & 114 & 32 \end{bmatrix}. \tag{2.3}$$

There is obviously endless ways to adjust the outcome in a way that makes the resulting image suit the particular aims. One way to advance the process is to use histograms that count how many of each greylevel there is and adjust the output to have more or less contrast, or darken or lighten the image. When working with 3D images the best way is to not adjust using histograms of each slice, as these may make the images notably varied from slice to slice. The simple algorithm will keep the outgoing images simple and consistent. Using a combined histogram for all the slices can be an adequate solution though. When converting to a scale with less greylevels, some information is bound to get lost in the process. In this case, 16bit greyscale has 65536 levels while 8bit is restricted to 256 levels. Because the contrast has been adjusted the rest of the processing will not be affected greatly.

Table 2.1: Tables to illustrate the change in greyscale when going from 4 bit greyscale (left table) to 2 bit (middle table) and downsizing pixels with a scale of 0.5 (middle to right table).

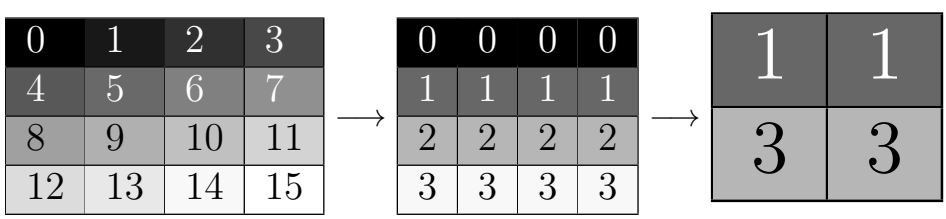

To further minimize the data downsizing the pixels is the next logical step (table 2.1, second arrow). The goal is to reach b number of pixels instead of the original a number of pixels. To ensure no distortions appear in the image reconstruction, one needs to scale all directions equally i.e. $b_x = s * a_x$, $b_y = s * a_y$ and $b_z = s * a_z$. For optimal results, it should be possible to scale with any constant, but the resulting scaled image cannot have a non-integer number of pixels. To deal with this most programs use some type of linear interpolation, in the case of ImageJ bilinear interpolation was used because it is applied to two dimensional images.

Combining sets of images

When imaging biological samples there is a possibility that more than one scan is needed to cover the entire sample. To solve this, a method for digitally merging them is necessary. There are many different solutions for this, where the Fourier Shift Theorem is one. FST uses phase correlation to find the optimal overlapping point between two different sets [21]. Implementations of this method also uses non-linear blending techniques to even out the final output. One implementation of the method was constructed by S Saalfeld et al., The Big Stitcher, is available as a plugin for ImageJ.

2.5.2 Thresholding

To convert a greyscale or coloured image to a binary image, a threshold can be used to separate the pixel values into two groups. This value can be arbitrarily chosen or more advanced methods can be used to find the optimal partition. The reason for thresholding is usually related to segmentation of the image.

Otsu's method

A common algorithm for optimal threshold computation is Otsu's method which uses probability to find an optimal parting so that the most prominent object within the image is separated by the binarization. To find the objects within the image every partition of the greyscale is tried. For every partition, the intraclass intensity variance is computed and the threshold that minimizes this is the one that will be the chosen partition of the greylevels. This process results in the optimal threshold. Otsu's method can be used to find more than one object by dividing the greylevels into more than two groups [22].

2.5.3 Filters and histogram equalization

There are many different methods for which images can be changed to give more information about the imaged subject. Filters and other methods can be used to remove noise or to enhance different areas. A median filter computes the center value of a window, most commonly a rectangular or square window with an odd numbered side length such that the center is one single pixel although a center of two or four pixels

are also possible [23]. The median filter is one of the most commonly used filters in image processing because of its efficiency in removing noise of different types (e.g. salt and pepper, Gaussian) and because of its simple implementation [24] (figure 2.7a median filtered on 2.7b).

To improve image contrast without changing the structural information in an image, a contrast enhancement method called CLAHE (Contrast Limited Adaptive Histogram Equalization) can be used (figure 2.7b is CLAHE filtered in 2.7c). By dividing the pixel intensities into bins, and by adjusting this histogram, the image is changed [25] (example of difference: figure 2.8). Compared to AHE (Adaptive Histogram

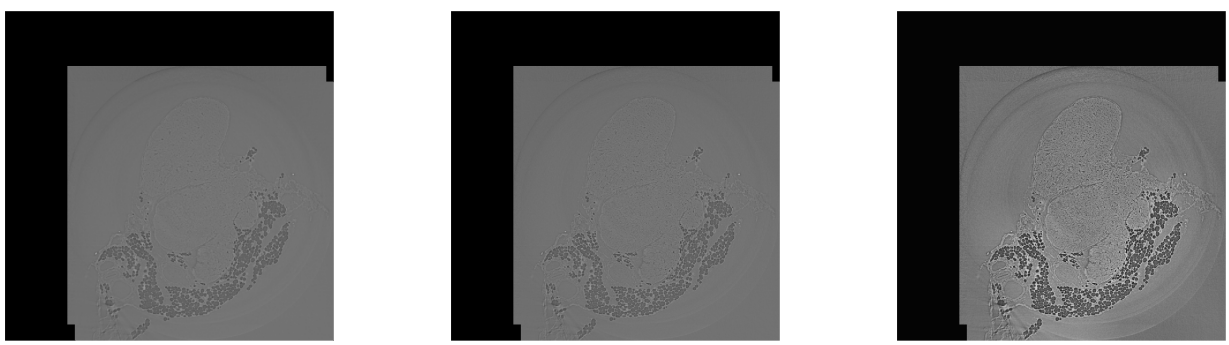

(a) Median (b) Original image (c) CLAHE

Figure 2.7: Example of the median and CLAHE operations on an image from the data set.

Equalization) CLAHE has a lower rate of overenhanced noise. This is because CLAHE equalizes histograms locally (in what is called tiles) in the image instead of a global equalization like the AHE [26]. This performance gain comes at a cost of finding the right input variables for the specific type of image, selecting for example number of bins and tile size for tiles [26]. In a study by Pisano et al. [25] by using CLAHE there was a statistically significant improvement in detection of possible tumors in mammograms. In another study by Joseph et al [26] the choices of variables and their effect on the output was thoroughly examined and CLAHE was shown to greatly enhance features of MR images with the right inputs.

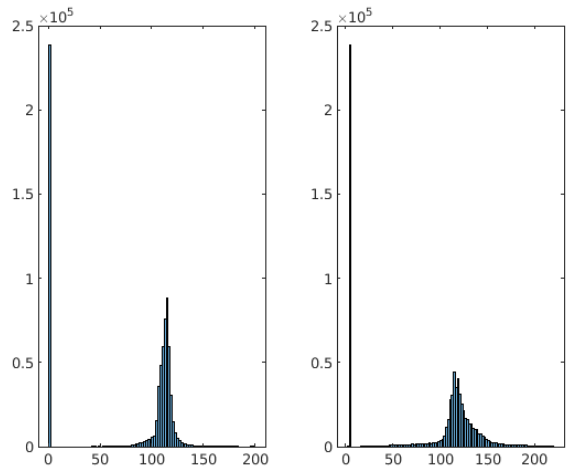

Figure 2.8: Histogram of an original image(figure 2.7b) and CLAHE image (figure 2.7c).

2.5.4 Morphological image operations

To increase the accuracy of the object extraction it is useful to adjust the edges of the objects. There are two basic morphological operations, erosion (figure 2.9a) and dilation (figure 2.9b). These operations are in the figures presented as an operation on binary images, where the dark blue is the original and the light blue is after morphological operation, although these morphological changes can be applied to any greyscale and even RGB image. How does the morphological image adaptation work then? A structuring element is chosen to either erode (dissolve) or dilate (expand) the edges of the object. In the figures (2.9 and 2.10) a circular structural elements have been used to illustrate the processes, but structuring elements can have almost any shape as long as it can be represented as a matrix. By doing this conclusions can be drawn on how well the chosen structure fits in to the image which depends on the objects edge features. A tendon and also a mineral mainly have rounded edges so a circular or spherical element is often suitable.

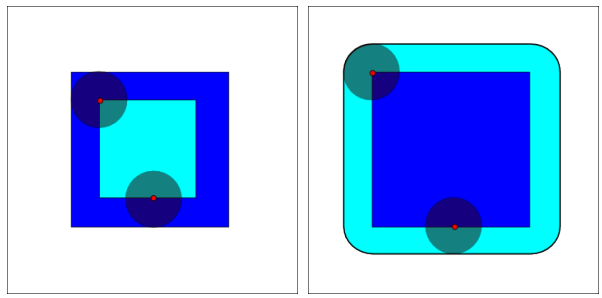

(a) Erosion [27] (b) Dilation [28]

Figure 2.9: The basic morphological image operations. Dark blue is the original image while light blue is after the operation has been performed.

By combining erosion and dilation in sequences, new morphological operations can be produced. The operation 'closing' is first dilating and then eroding using the same structural element (figure 2.10a), and the operation 'opening' is eroding and then dilating (2.10b). Smoothing inner corners outwards and outer corners inwards, as the figure shows, is a useful way to isolate background of objects so that they can more easily be extracted.

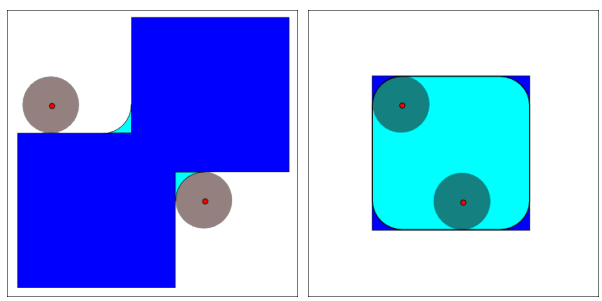

(a) Closing [29] (b) Opening [30]

Figure 2.10: The more complex morphological image operations.

Chapter 3

Materials & methods

3.1 Material

This section explores the methods used to produce the data explored in the thesis. The work has been performed by other people, the animal testing has been lead by Dr. Malin Hammerman and the synchrotron x-ray work has been performed by Dr. Maria Pierantoni.

3.1.1 Animal model

The image data consisted of images previously obtained from two studies. Study one included 14 female Sprague Dawley rats aged 10-12 weeks at the beginning of the experiment. The rats were then divided into two groups at random where the first group, *FL*, underwent normal full loading by being subjected to normal cage activity and the second group, *UL*, had their right leg paralyzed by a botox injection and their joint fixed using an ankle foot orthosis so that no movement of the lower leg was possible [2], [31]. After four weeks the rats were euthanized and the tendon along with the muscle complex and the calcaneal bone were separated from the rest of the body. The tendon complexes were placed individually in a phosphate buffed saline solution and frozen at -20° C for storage.

The second study was done in a similar way, nine Sprague Dawley rats aged 10-12 weeks were randomly separated into three groups to experience different amounts of microneedling damage into the right tendon. Three rats were needled 0 times and used as a control group, three were

needled 5 times and three were needled 20 times. The needling was done by piercing the skin at four different points of the right leg, one on each of the lateral (from the outer side), medial (from the inner side), proximal (from the top) and distal (from the bottom) sides. From each of these points the needle was pressed in five directions to create 20 microinjuries. For the 5 times needled this was done in the same way as for the 20 times needled but only on the lateral side of the tendon. The rats experienced normal cage activity. After four weeks the rats were euthanized and the needled tendons were harvested and stored in the same way as the first study. Similar animal models are described in Hammerman et al [2] and Pierantoni et al. [6] in more detail.

The animal experiments were performed by Dr. Hammerman and were approved by the regional ethics committee in Linköping. The experiments adhered to the institutional guidelines of treatment and care for laboratory animals.

3.1.2 Phase contrast enhanced X-ray tomography

The imaging was done as described in a paper by Maria Pierantoni et al. [6]. The goal was to image the subtle differences in contrast between the collagen fibers and the surrounding matrix. Samples from the animals were preserved freshly frozen in PBS (Phosphate Buffed Saline solution) and mounted inside Eppendorph tubes. The calcaneal bone of each sample was glued to the lid of the tube and the muscles were placed in the tip of the tube so the sample would be fixated. The tubes were then easily mounted into a special sample holder at the beamline. The experiments were performed at Swiss Light Source at the Paul Scherrer institute using the X02DA TOMCAT beamline. To improve the phase contrast in the images the distances within the optical setup was optimized as well as the X-ray energy level. In addition a HNAM , *High Numerical Aperture Microscope* was used to achieve the high resolution of $1.63 \times 1.63 \times 1.63 \mu m^3$ per voxel (*volume pixel*). The samples from the first set (fully loaded and unloaded set) were imaged in two sets which meant that the heelbone and muscle complex was not always included in the image sets for all samples. The samples from the second (needled) set were imaged in three sets which together had both the heelbone and the bottom of the muscles present.

3.2 Methods

The process of analysing the image sets were the main task in the thesis. It can be divided into the preprocessing steps and the segmentation process. Most of the preprocessing steps were done in ImageJ, with exception for the 8-bit conversion, whilst the binarization exclusively was executed in MATLAB.

Mainly MATLAB and ImageJ has been used to achieve this. ImageJ is largely a visual program, it is a useful tool to visualize 3D image volumes by displaying it in slices of any direction which are easily scanned through. Furthermore it is a great asset for assessing the different stages of the image adaption process. MATLAB has been used to filter and convert the images and to automatically segment the soft tissue and mineral.

3.2.1 Preprocessing steps

Because of the size of each data set the data was preprocesed. This was done in a few different ways. The preprocessing would make the the data a bit more coarse, but the effect on the final output deemed small. To reduce the data size of each 3D image set the, data was preprocessed in a few different ways. First, the 16bit images was downsized to 8 bit.

To further minimize the data the number of image voxels was also scaled down. To not lose too much data it is desired to keep the pixels as small as possible. In the end the scaling factor was set as 0.33 in all directions. Ideally all samples were first scaled by 0.33 in all directions and then stitched, but because of how future steps of the process works some samples were first only scaled by 0.33 in the x and y direction while the z direction was scaled with 0.50 or 0.66, depending on the sample. This made the stitching possible for almost all samples. After stitching these samples, they were then scaled down again by 0.5 or 0.66 (depending on the original scaling factor, mathematically: $0.5 \cdot 0.66 = 0.33$) so that the entire downscaled sample had a homogeneous pixel size in all directions.

To combine the image sets of each sample stitching was done to combine the sets into one 3D representation of the tendon (figures 3.1a and 3.1b). The stitching was done using the Big Stitcher plugin of ImageJ. Some samples only had one data set of interest and of adequate quality

and thus did not require any stitching, but most had either two or three sets to be put together. When stitching three sets, a method that could be called 'three-time-stitching' was used. This meant first stitching set A and B, creating AB, then B and C, creating BC. Then stitching AB and BC to get the final ABC. This shown to be a little more successful than stitching A and B to get AB and then AB with C to get ABC.

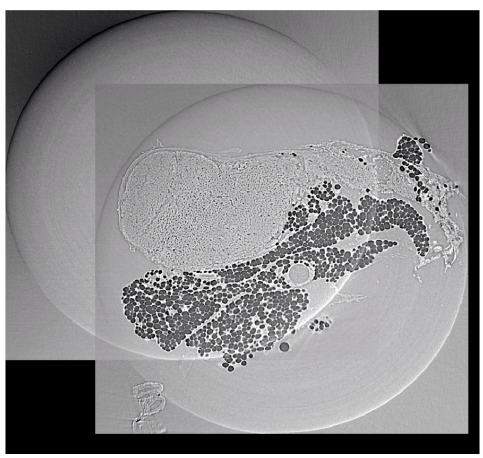

(a) An example of two stitched sets in the z-plane.

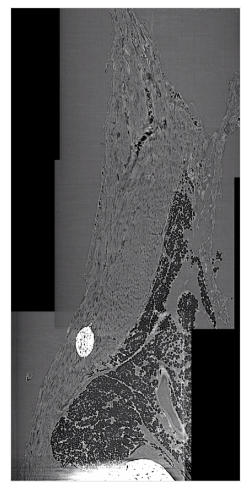

(b) An example of three stitched sets as a longitudinal view.

3.2.2 The segmentation process

To both segment out the mineral and the tendon, a tissue binarization code was done separately. Some operations were developed on the 3D stack while some operations were done on 2D slices, most commonly in the cross sectional z-direction.

Mineral

Because the mineral is highly contrasted compared to the surrounding tissue, the segmentation was rather straightforward. Binarization was executed with threshold level 0.80 (level ranged from 0 to 1) (figure 3.2b). This threshold was chosen based on the fact that hard tissue, such as the mineral, appear with a high greylevel near white (which has level 1). This in combination with a process of trial and error gave the mineral threshold value. After this, morphological steps were taken to remove small white speckles from tissue, separate from the minerals, salt

and pepper noise and artefacts from the image taking process. These first included opening and closing with a 3D cuboid elements with sides 2, 2 and 10 (figure 3.2c and 3.2d). After this all existing holes were filled (figure 3.2e). Continuing with morphological operations included opening and closing the individual slices in the z-direction (cross sectional direction) with a circular structural element with radius 3 pixels (3.2f and 3.2g). Lastly, code to fill all holes were used again on each z-slice (figure 3.2h). The voxels that now remained were examined on how they connected to each other using the in MATLAB. Voxels were considered part of the same component/object if they connected in one of 26 ways along one of the 6 faces, 12 edges or 8 corners of the voxel cube. From the final connected components volume and placement data was extracted. Lastly the final binary segmentation was multiplied with the ingoing 3D image to produce a masked image (figure 3.2i).

Tendon

Compared to the mineral the other tendon tissue is more similar in greylevel to the surrounding tissue background. First to remove some noise, a median filter was applied (figure 3.3b). To combat the similarity in greylevels a CLAHE filter was applied on every individual cross sectional slice (figure 3.3c).

After enhancing the contrast and removing the noise the next step was to remove the fat tissue that surrounds the tendon. This was done for every cross sectional slice. The intensity of the fat was low compared to the soft tissue of the tendon (see for example figure 3.1b), but the fat usually have a lining that appears due to the phase contrast method which has a higher contrast similar to the tendon tissue contrast level. The fat was easily identified using binarization with level 0.36 (on a scale from 0 to 1). This also included black background that appears as an artefact from the stitching (figure 3.3d). The identified fat and black background was then changed to the general grey background of the image (figure 3.3e). The grey background value of the image was taken as the median grey value of the entire 3D image (figure 3.3f). The lining was removed in a later step. After the fat was removed the non black background was to be removed (figure 3.3g). This had a simple implementation of opening with a 6 pixel wide disc element at every slice and then subtracting this result from the original image (figure 3.3h).

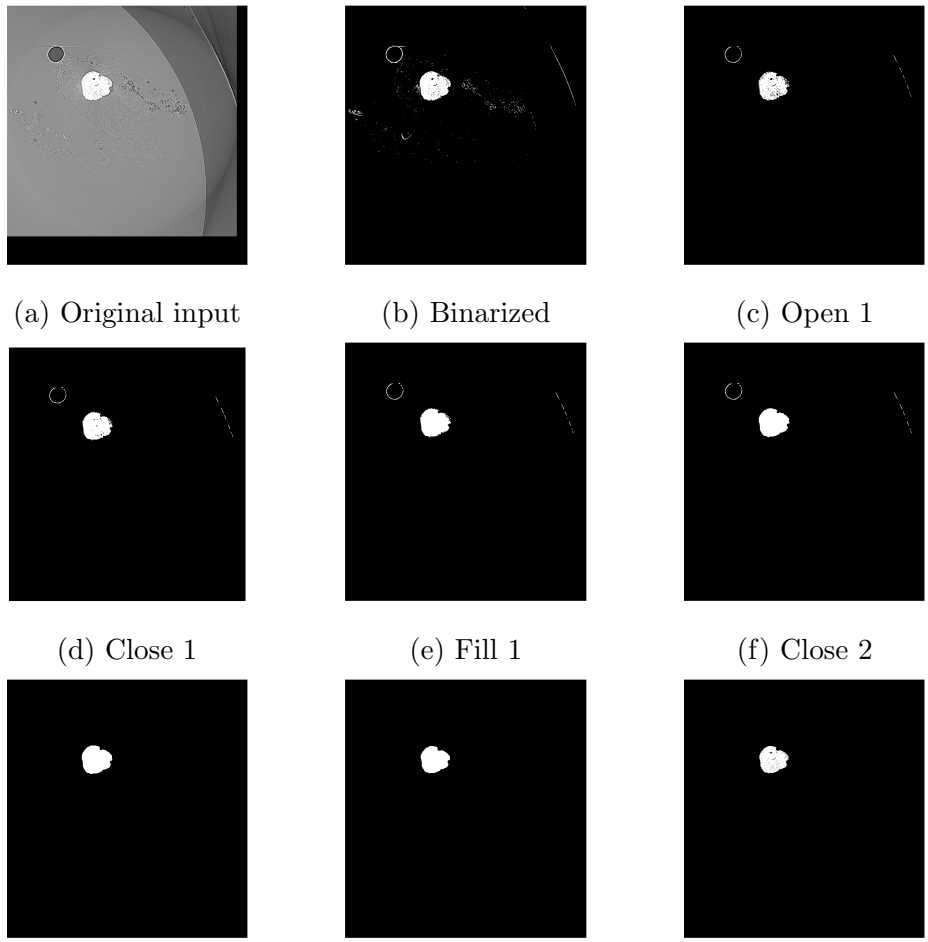

(a) Original input (b) Binarized (c) Open 1

(d) Close 1 (e) Fill 1 (f) Close 2

(g) Open 2 (h) Fill 2 (i) Masked

Figure 3.2: The complete steps of the mineral pipeline.

Binarizing was done using the optimized threshold method designed by Otsu [22] (figure 3.3i). The binarized image was then morphologically closed and opened using a circular elements with radius 3. This was done to remove the lining of the fat. After this a flood fill function was used to fill the holes for every cross sectional slice. To improve the segmentation further the procedure of morphological operations and flood filling of holes was done in eight more steps using different structural elements (adding up to 12 morphological steps in total), in this case cuboids and discs (figure 3.3k).

In addition to the previously described steps the object identifying function *bwconncomp* is also used here to extract only the largest object in the 3D image. Lastly a masked version is produced from the original tendon image and the binarized segmentation (figure 3.3l). This is simply done by multiplying the binary image with the original turning all pixels not part of the segmentation black and all segmented into the original grayscale.

3.2.3 Extraction and processing of segmentation data

From the final segmentations data to compare the different sets can be extracted. These steps were all done using MATLAB.

To find the volume of the tendon and the minerals counting the white pixels of the segmentation is the most straight forward solution. This was done measuring the length the pixel index list from the largest component in the segmentation for the tendon and for any component larger than 150 pixels for the mineral extraction. This was acquired from the function *bwconncomp* in MATLAB which finds all connected components in a specified image. To establish the real world volume the pixel volume is multiplied with the voxel size, $1.625 \times 1.625 \times 1.625 \mu m^3$.

The number of heterotopic ossifications (HO) in each sample is of interest as well as their placement in relation to the calcaneal bone and the calf muscle complex more than the exact metric position, which is dependent on the length of the tendon. The normalized placement with the end of the calcaneal bone at 0 and the start of the muscle complex at 1 will give a comparable number for all tendons. Since only the mineral is of interest the computational time can be reduced by selecting a smaller number of slices that surround all the minerals of a tendon. Using *bwconncomp* again after the segmentation and calling a command (*centroid*) gives us the midpoint of each connected component (in this case each mineral). This number is relative to the start of the mineral segmentation image, i.e. the first slice of the mineral segmentation. To get the actual placement in comparison to the calcaneal bone adding the difference in slice number between the end of the calcaneal bone and the beginning of the mineral set is necessary. This number is then

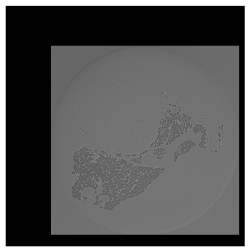

(a) Original input

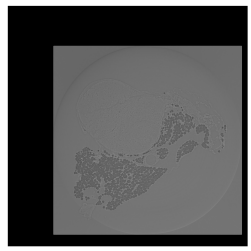

(b) Median filtered

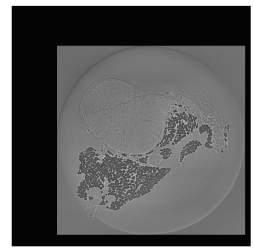

(c) CLAHE

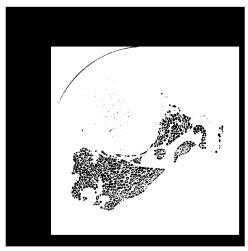

(d) Fat binarization

(e) Fat adjustment and complement

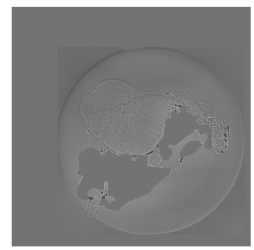

(f) Fat removed

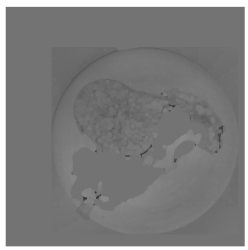

(g) Back identification

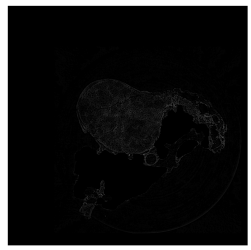

(h) Tendon without back

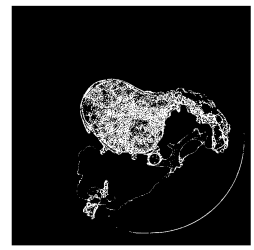

(i) Binarized without back

(j) Morphological steps

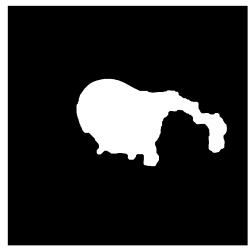

(k) Final segmentation

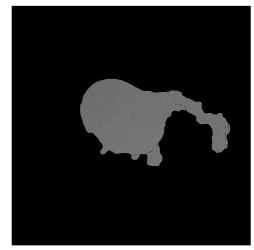

(l) Masked

Figure 3.3: Selected steps from the tendon segmentation pipeline.

normalized by the difference between in slice number between the cal-

caneal bone end and the muscle complex start.

For some samples it was not possible to stitch the tendons, to solve this the individual 3D images were run separately through the segmentation processes. To still obtain accurate data from these special calculations had to be supplied. Volumes were added to each other after all the segmentations were finished. For samples where the mineral was cut in between two 3D images, the centroids were computed, in the way that was explained previously, for both 3D images and the placements where then weighted against the volume of the mineral to find the shared midpoint of the two parts. This was only done in the z-direction because the x- and y- directions were of no interest.

Chapter 4

Results

For all graphs presented in this results chapter the different sample preparation methods have been grouped separately. The same procedures for analysing data has been applied to both the unloaded and fully loaded tendons as well as the needled tendons and their control.

4.1 Comparing unloaded and fully loaded tendons

4.1.1 Tendon segmentation

From the tendon segmentation the total tendon volume could be calculated. The average volume and the standard deviation of it can be seen in table 4.1 for both the unloaded (UL) group and the fully loaded (FL) group. The groups appear in a similar range between $5mm^3$ and $20mm^3$ (figure 4.1).

Table 4.1: Averages and standard deviations of total tendon volume for the unloaded and fully loaded samples.

	Average	Standard deviation
UL	$13.8mm^3$	$4.2mm^3$
FL	$11.0mm^3$	$4.8mm^3$

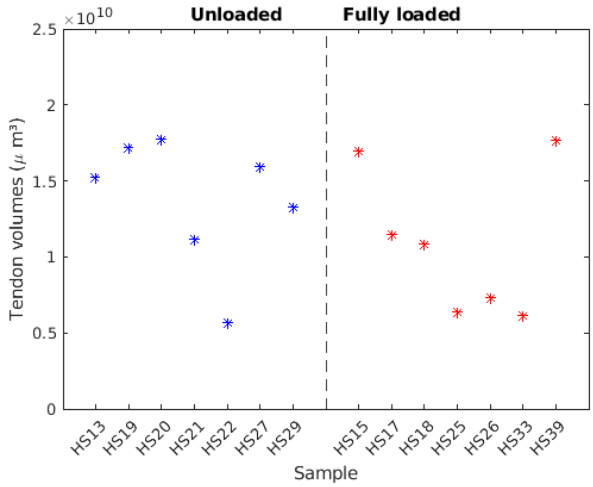

Figure 4.1: Tendon volume for different samples. All samples that went under the full loading regime have the colour red in all graphs, the unloaded have blue.

4.1.2 Mineral segmentation

For the mean and standard deviation calculations of the mineral volume and placement, one sample, HS21, was left out since this sample did not have a mineral present in the imaged tissue. This sample is still shown in the graphs though.

For both the unloaded and the fully loaded group all heterotopic ossifications were located in the lower half of the tendon. The number of heterotopic ossifications for the unloaded group varied between zero and three whilst the fully loaded group had between one and six ossifications (figure 4.2). The average placement and standard deviation for the different groups is shown in 4.2 The volume for each mineralization

Table 4.2: Averages for the unloaded and fully loaded groups of the normalized mineral placement compared to the tendon length.

	Average	Standard deviation
UL	0.1605	0.0999
FL	0.2912	0.1261

as well as the total volume for all heterotopic ossification in a sample could be computed in a similar way as the tendon volume. The indi-

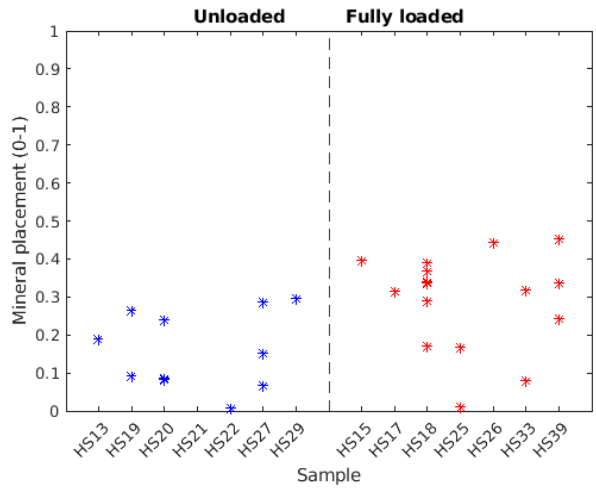

Figure 4.2: The normalized mineral placement compared to the tendon length. At 1 is where the insertion of the muscles start and 0 is where the heelbone is located.All samples that went under the full loading regime have the colour red in all graphs, the unloaded have blue.

vidual and total mineral volume means for the two different groups is displayed in table 4.3 (figure 4.3, the total volume is shown as a circle above the individual mineral volumes or around the one sole mineral volume for the samples only containing one mineral).

Table 4.3: Averages for the total and individual mineral volume for the different samples of the different loading groups.

	Average	Standard deviation
UL total	$0.15mm^3$	$0.14mm^3$
FL total	$0.06mm^3$	$0.04mm^3$
UL individual	$0.08mm^3$	$0.10mm^3$
FL individual	$0.03mm^3$	$0.04mm^3$

The amount of mineral compared to tendon in volume was also examined. For both groups the mineral volume did not override 2.5% of the total tendon volume (figure 4.4). The mean and standard deviation for the groups is displayed in table 4.4

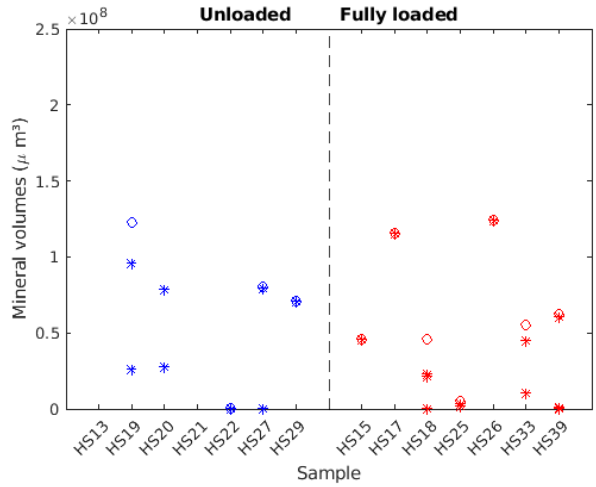

Figure 4.3: The mineral volume for the different samples of the different groups, total volume for each sample is displayed as a circle and individual volumes are marked with a star. All samples that went under the full loading regime have the colour red in all graphs, the unloaded have blue.

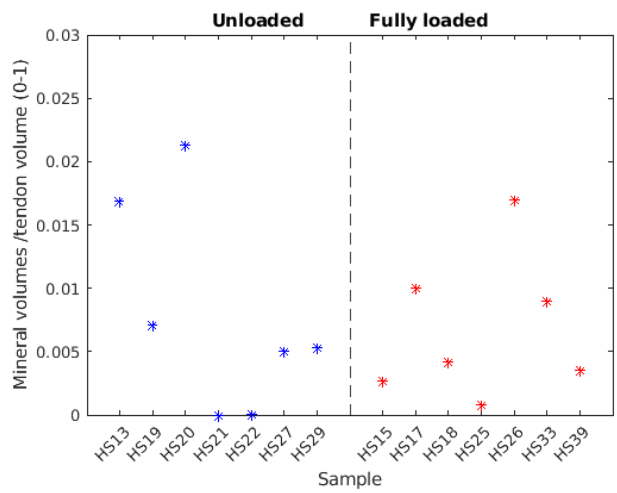

Figure 4.4: The ratio of mineral volume over tendon volume for the different groups. All samples that went under the full loading regime have the colour red in all graphs, the unloaded have blue.

Table 4.4: Average and standard deviation of the mineral volume over the tendon volume for the unloaded and fully loaded groups.

	Average	Standard deviation
UL	0.0078	0.0080
FL	0.0067	0.0056

4.2 Comparing tendons microdamaged by needling

For the needled sets the control group (needled 0 times) are in green, needled five times is black and needled twenty times is magenta.

4.2.1 Tendon segmentation

For the microinjured groups the average tendon volume and the standard deviation are displayed in table 4.5. The volumes ranged between $11mm^3$ and $21mm^3$ (figure 4.5).

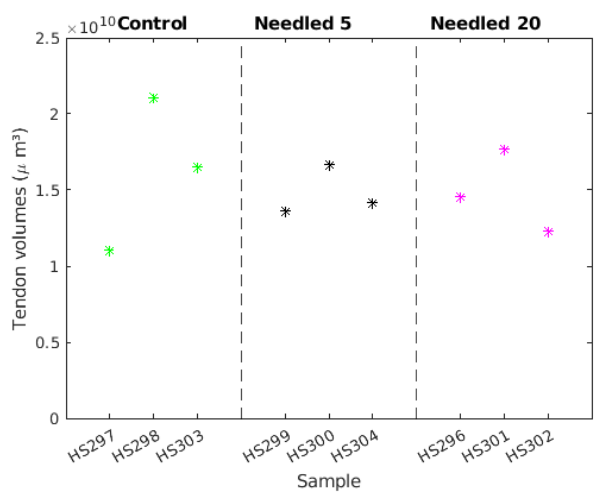

Figure 4.5: Tendon volume for different samples. For the needled sets the control group are in green, needled five times is black and needled twenty times is magenta.

Table 4.5: Averages and standard deviations of total tendon volume for the needled 5 and 20 times and the control group.

	Average	Standard deviation
Needled control	$16.2mm^3$	$5.0mm^3$
Needled 5 times	$14.8mm^3$	$1.6mm^3$
Needled 20 times	$14.9mm^3$	$2.7mm^3$

4.2.2 Mineral segmentation

Position of the mineral for the needled sets and their control were similar. For the different groups the means and standard deviations are displayed in table 4.6. For all of these samples the mineral appeared in the lower half of the tendon (figure 4.6).

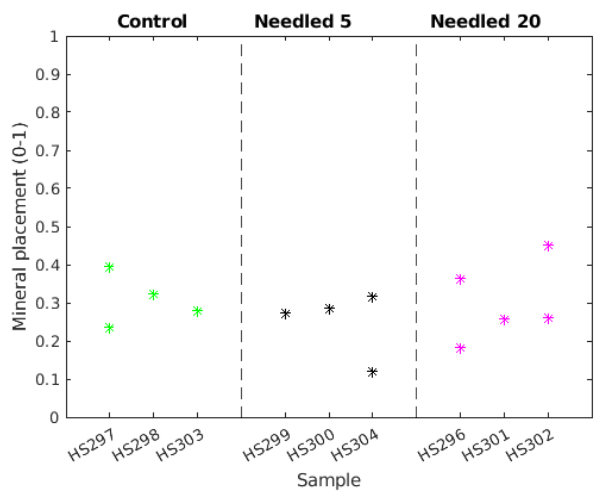

Figure 4.6: The normalized mineral placement compared to the tendon length. At 1 is where the insertion of the muscles start and 0 is where the heelbone is located. For the needled sets the control group are in green, needled five times is black and needled twenty times is magenta.

The volume for each mineralization as well as the total volume for all heterotopic ossification in a sample could be computed in a similar way as the tendon volume. Compared to the placement of the mineral the different testing groups have a larger differences, in general the two needled sets have higher volumes on individual heterotopic ossification and

Table 4.6: Averages for the needled 5 and 20 times and the control group of the normalized mineral placement compared to the tendon length.

	Average	Standard deviation
Needled control	0.3076	0.0677
Needled 5 times	0.2495	0.0890
Needled 20 times	0.3037	0.1046

on the total mineral volume. In table 4.7 the averages and standard deviations are shown for both the individual volume and for the total volume and for all samples (figure 4.7).

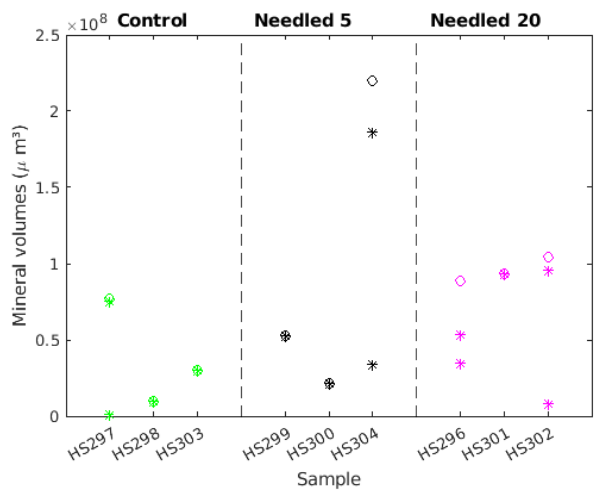

Figure 4.7: The mineral volume for the different samples of the different groups, total volume for each sample is displayed as a circle and individual volumes are marked with a star. For the needled sets the control group are in green, needled five times is black and needled twenty times is magenta.

For ratio between mineralization volume and tendon volume all samples but one were below the 1% mark. The control and the needled 20 time set had quite small variation between the tendons in their group whilst the needled 5 times has a clear larger outlier (figure 4.8). The average and the standard deviations for the ratio is displayed in table 4.8.

Table 4.7: Averages for the total and individual mineral volume for the different samples of the needled 5 times and 20 control group.

	Average	Standard deviation
Needled control total	$0.04mm^3$	$0.03mm^3$
Needled 5 times total	$0.10mm^3$	$0.11mm^3$
Needled 20 times total	$0.10mm^3$	$0.01mm^3$
Needled control individual	$0.03mm^3$	$0.03mm^3$
Needled 5 times individual	$0.07mm^3$	$0.08mm^3$
Needled 20 times individual	$0.06mm^3$	$0.04mm^3$

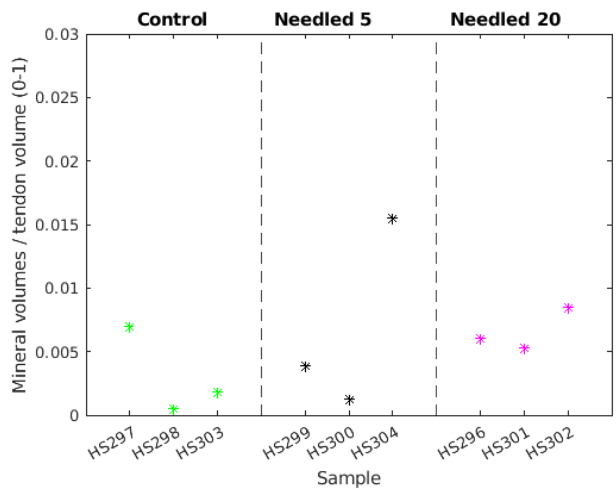

Figure 4.8: The ratio of mineral volume over tendon volume for the different groups. For the needled sets the control group are in green, needled five times is black and needled twenty times is magenta.

Table 4.8: Average and standard deviation of the mineral volume over the tendon volume for the needled 5 and 20 times groups and the control group.

	Average	Standard deviation
Needled control	0.0031	0.0034
Needled 5 times	0.0069	0.0076
Needled 20 times	0.0066	0.0017

4.3 Tendon volume renderings and mineral morphologies

To illustrate how the tendon (figure 4.9) and mineral (figure 4.10) segmentation processes performed, the original images has been masked using the resulting segmentation.

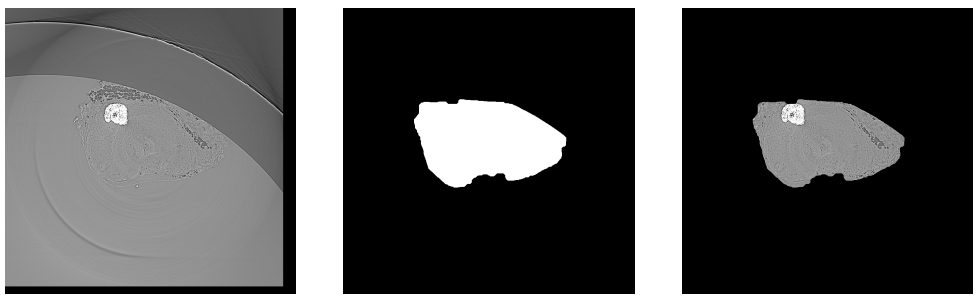

(a) Original (b) Binarized (c) Masked

Figure 4.9: Cross sectional view of the segmentation of tendon taken from sample HS19 from the unloaded dataset.

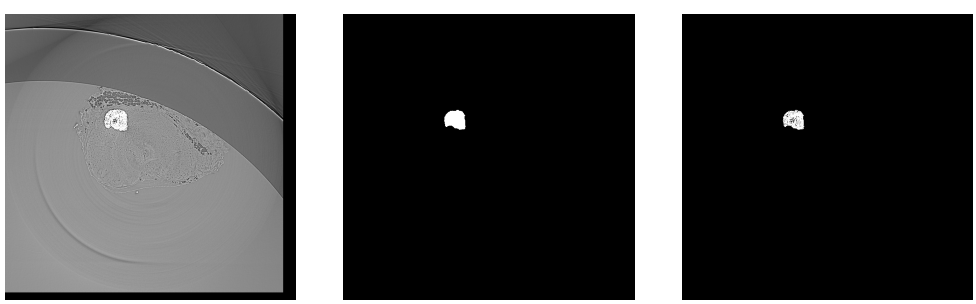

(a) Original (b) Binarized (c) Masked

Figure 4.10: Cross sectional view of the segmentation of mineral taken from sample HS19 from the unloaded dataset.

Longitudinally it is easier to evaluate the consistency of the segmentation of the tendon (figure 4.11). This way it is possible to observe more problematic areas for segmentation as well as defects in the process. Problematic areas can for example be places where there is soft tissue on multiple sides of fatty areas, this can be seen in the upper half of figures 4.11a and 4.11b. There is also parts of individual smaller tendon bits that appear separate from the longitudinal slice seen in 4.11b but

these pieces are connected to the larger segmented object through other slices.

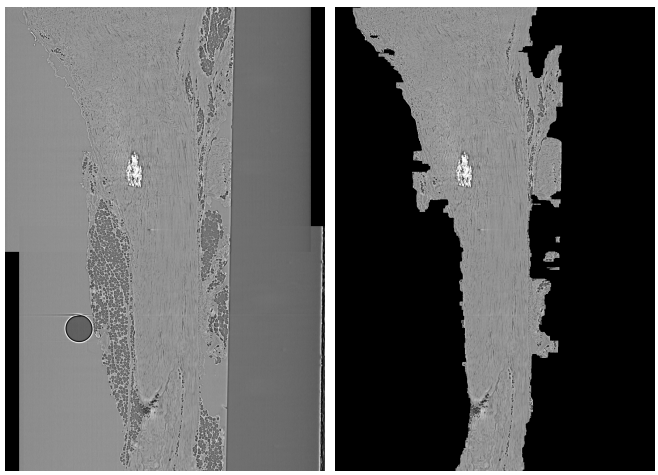

(a) Orginal (b) Masked

Figure 4.11: Longitudinal view of the segmentation of the tendon taken from sample HS19 from the unloaded dataset.

In some cases the segmentation of the mineralizations got problematic because of thin connections between two larger bodies, examples of this can be seen in figures 4.12 and 4.13.

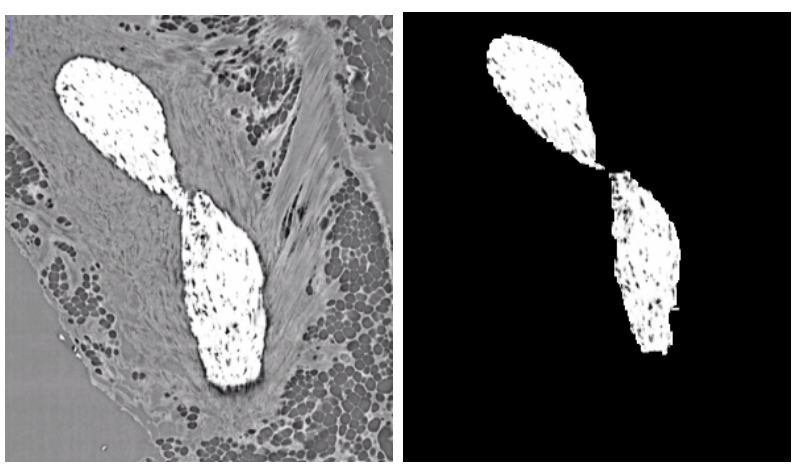

(a) Original (b) Masked

Figure 4.12: Longitudinal view of the mineralization of sample HS19.

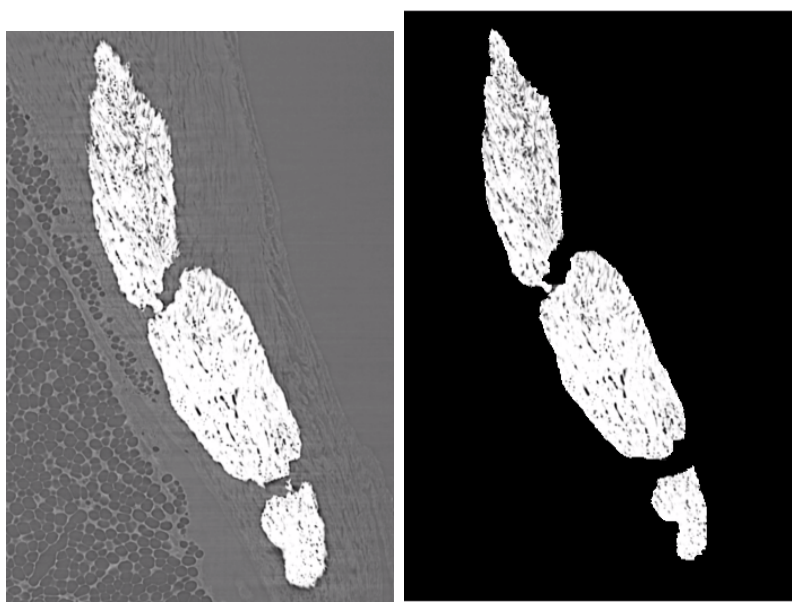

(a) Masked (b) Masked

Figure 4.13: Longitudinal view of the mineralization of sample HS304.

Chapter 5

Discussion

The goal of this thesis was to investigate the occurrence of heterotopic ossifications within the intact rat Achilles tendon in response to different loading and microinjuries. This was done by image analysis of high resolution images obtained by phase contrast enhanced tomorgaphy. Segmentation was done on the whole tendon and the mineral tissue inside the tendon. This produced results relating to the volumes and placement of the minerals which will be discussed in this chapter along with the processes used in this thesis.

5.1 Interpretation & differences in data-groups

Analysing the data presented in the results section the observation is made that the different groups are highly similar in many regards. For much of the data the testing groups and the control had similar averages but in many cases the standard deviation was larger for the control groups. In relation to this, it is possible that there were some effect observed from the testing. Because of the small amount of samples in each test, seven for the unloaded and its control respectively and three for each of the needled sets and their control, it is difficult to say something for sure. Most statistical test require a higher amount of samples.

When looking at the total tendon volume there were no clear differences in the unloaded and the fully loaded sets. They had somewhat different averages, but their standard deviations are large enough to include the other groups average. The unloaded group seem to generally

have larger volume than the fully loaded, but the spread is large for both groups. Both groups had samples who had three times larger volume than other samples within the same group (figure 4.1). However the large differences in samples could be due to one specific limitation of this study. In fact, for a few specimens, it was not possible to image the whole tendon and its extremities. For these some length, and in extension volume, was lost. This can shed some light on the differences between the needled groups and the unloaded and fully loaded groups. The needled sets and their control had generally a higher mean volume than the unloaded and fully loaded sets. The standard deviations were also smaller for the two needled test groups the coefficient of variance (std/mean) was for these two 11% (needled 5) och 18% (needled 20) and for the other groups they were 31% (needled control), 30% (unloaded) och 44% (fully loaded). This marks how close all the points of the two needled sets are compared to the control set (figure 4.5).

An interpretation of this would be that the two needled groups are more homogeneous than the control. All of the animals were subjected to normal cage activity after needling or no needling. There is no record of how the animals behaved after the procedure, but there is a possibility that the needled animals behaved more similar to each other than the control group because of their injury. The control group had no problems behaving normally, which can have made their tendons thicker, and then it is just individual activity level (and genes) that decides the thickness of the tendon, i.e. more natural variation. Loading at different levels may affect the shape of the tendon [1]. However this is not observed in the unloaded and fully loaded sets. The unloaded tendons had a tendency of being larger than the fully loaded ones, the difference between the means were $13.8 - 11.0 = 2.8mm^3$. This is supported by another study that found the cross sectional area to be similar in both tendons that had been unloaded using botox and the control tendon [31]. This was a bit of a surprise since they also observed an increase in collagen content of the unloaded tendon.

In the unloaded group the individual mineral volume as well as the total mineral volume is not consistent between different tendons. The coefficient of variance for these were respectively 125% with mean $0.08mm^3$ and 93% with mean $0.15mm^3$. This could be because of biological variation. Note that tendon HS21 has not been included when computing

the mean and standard deviation for this group. The fully loaded group also vary much, but the mean was much lower especially in the total heterotopic ossification volume, coefficient of variance 133% and mean $0.03mm^3$ for individual and 67% and $0.06mm^3$ for total. For the needled groups the total volume is very consistent for the needled 20 times group with a coefficient of variance at only 10%. The needled 5 times group has one large outlier which is HS304 that contains three larger minerals which makes its coefficient of variance for the total volume 110%. Lastly for the control group the coefficient of variance was 75% for the total volume.

The ratio of heterotopic ossification volume compared to tendon volume was $0 - 2.5\%$ in all cases. There was not much difference between the unloaded and the fully loaded group. The needled groups and the control had some interesting differences though. Control has a much lower mean while the two needled groups have similar values, 0.31% versus 0.69 and 0.66. The needled 20 times group also has a low standard deviation (0.17%) while the other two groups have standard deviations in the same range as their means, 0.34% and 0.76%. The coefficient of variance was 109% for control, 110% for needled 5 and 26% for needled 20. This indicates that needled 20 is a group that had very similar responses, while needled 5 seems to be in between this and the control group, which the testing method also is.

The number of heterotopic ossifications did not increase with the total mineral volume, for example samples HS27 and HS29 have similar mineral volume but HS27 had two heterotopic ossifications where HS29 only had one. There were generally a similar number of mineralizations for all groups, generally one, two or three, but the mineralizations tend to be larger for the needled groups. This is somewhat counterintuitive since one would hypothesize minerals appear at the sites of microinjuries which was not really the case here. When observing the raw samples the tendons seem to not correlate with the mineral placement, most are placed somewhat near the middle of the tendon. In an article by Lin et al. [3] they mention that heterotopic ossifications always have been modeled using animal models with trauma to the tendon. They however observed that the contralateral tendon of an injured tendon had a spontaneous development of mineralization. This in combination with what has been observed in this thesis makes it seem that the key point of the

mineralization is not necessarily the trauma but something else. Lin et al. suggest that it is the overloading of the tendon that contributes to the formation of heterotopic ossifications [3]. This does not add up with the theory presented in a previous paragraph that suggests that the animals would load their injured legs less than the unharmed control group.

The mineral placement for the fully loaded and unloaded groups were all in the bottom half of the tendon (figure 4.2). The unloaded set have a more compact range compared to the fully loaded (standard deviations 0.0999 and 0.1261 respectively), which again might point at the larger variation in cage activity in the fully loaded group compared to the restricted unloaded group. Looking at the number of minerals, the difference is larger but there are outliers to consider. Unloaded group has a tendon without a mineral whilst the fully loaded group has a tendon with 6 minerals. Although, if the test sets were larger would we see more high outliers for the fully loaded group and more low outliers for the unloaded group? Instead look at the needled groups the difference is less between all the groups both regarding placement and number. Comparing the needled control with the fully loaded group though, as theoretically they are the same, they have very similar average placement which is expected. One can again look at the article from Lin et al. [3] and say that this might indicate that ossifications are induced by intensive loading on the Achilles tendon under normal conditions. To add to this may in turn be related to microdamages since these can be caused by intensive loading. There is not however sufficient data from this study to say for sure, the group sizes are too small and also the intragroup variation is too large to make any final conclusion.

When observing the mineral segmentation and cross checking with their original image sets to confirm if the segmentation worked one could observe that in many tendons the heterotopic ossification looks like it was previously two and has thus grown together (figure 4.12 and 4.13). There are also samples where two heterotopic ossification are pointing towards each other as if they are tending towards growing together (not pictured). This is an interesting observation. If we assume the hypothesis discussed by Lin et al. [3] metabolically active cells are what promotes the growth of minerals, it is not unreasonable that where two different minerals are close the active cells will be in greater number. This is assuming the active cells stay around the mineral or are

connected to the mineral in some way. This mineral behaviour occurs across almost all groups, both unloaded and fully loaded as well as the needled 20 times group.

5.2 Resulting segmentation

The segmentation is not fully accurate as seen in the results. The segmentation was particularly problematic in the first and last slices of the segmentations. Each cross sectional slice is about $1.6\mu m^2$ which will not affect the final calculations greatly. This could be due to the usage of 3D elements in the segmentational process. A solution to this could be adding a few slices onto the beginning and end, which are later removed to exclude the muscle and heel. Excluding the 3D elements could also be a solution, but the improvement these 3D elements give by introducing a consistency throughout the slices to the total segmentation outweighs the problems with the first and last crossectional slices.

Looking at figures 4.10 and 4.11 comparisons between a more realistic segmentation (by identifying the edges of the original tendon image) and the segmentation produced by the methods described can be made. Even though the fat is removed there are some other thin tissue that surrounds the tendon which becomes a problem when using the fill steps of the segmentation. This is also visible in the longitudinal view as the protruding parts (figure 4.11).

The mineral segmentation successfully removed white artefacts that appear from the imaging process (a type of this artefact is seen in figure 3.2). The mineral segmentation failed at certain smaller points such as small bridges between larger mineral pieces as well as other thinner areas such as the ends. This might be because of holes within the mineral pieces.

5.3 Preprocessing of raw data

The data this project has analyzed was not always suitable for the chosen processes which made parts of the process challenging. Both individual samples and whole groups had intrinsic imperfections. For many cases special methods were developed to overcome these prob-

lems and optimize the quality, and in some cases they were overlooked, finding solutions would be too time consuming. The accuracy of this preprocessing could be improved by further studies with these data sets.

As previously mentioned each tendon was imaged in two or three different segments. To achieve a consistent segmentation these segments were stitched together. For most tendons this worked fine and there was no problems, though for some the Big Stitcher did not to work. The main reasons for not being able to stitch seemed to be either that there were too few overlapping images or that the angle varied in between segments. For some samples the problems with too few samples were solved by scaling down in sequence.

For three samples, two from the unloaded and one from the fully loaded group, the stitching did not work even though many different processes to adapt them were tried. To still include them in the final data extraction their unstitched image sets were individually segmented and their volumes etc were added after this individual extraction. One, could because of this development, doubt the necessity of the stitching process since it did not work for all tendons. Alternatively to the method used here the stitching could be performed after the image sets had gone through the segmentation. This would put a quality restriction on the segmentation though which could be ruined by individual image sets composition like number of specific greylevels, using the two or three sets together gives a more unified binarization. The second option could be to remove the stitching entirely and use the special methods developed for the three unstitchable tendons for all. This solution could work but again the specific greylevel composition could affect the segementations. Intuitively though a visualization of the tendon that is obtained from the stitching is a great tool, it makes the understanding of the compositions and locations more clear.

A difficulty encountered during the segmentation was that almost all the fully loaded and unloaded sets did not include any slices containing the heel bone. This posed a problem for of the measurements for example the normalized mineral placement. For some tendons, namely HS22 and HS25, there was also a bit of ambiguity regarding if the mineral is actually parts of the calcaneal bone. For context, in these samples the 'mineral' is present from the first slice and they do not look like the end

of the calcaneal bone if compared to the other samples.

5.4 Image processing steps

Depending on the method of downsizing separating the different soft tissues can become a problem. Therefore it is important to monitor how the downsizing is done. There can also be issues with differences in grayscale between the slices of the image volume. If this occur the later procedures leading up to the binarization will get distorted and unrepresentative. In the end MATLAB was chosen to go from 8bit to 16bit because it was easier to monitor the process compared to ImageJ. The most basic method implemented in MATLAB was used but there are probably more appropriate ways to adjust the grayscale. For example, the intensity of the fat usually have a lining that appears due to the phase contrast method which has a grey colour. This lining could maybe have a more practical range of grayscale but using a more specific grayscale This was not researched very thoruoghly since the most basic version worked fine.

When adapting the images for the segmentation a mix of 2D and 3D methods were used. There was many different reasons for what was used. There was always a reflection regarding if 2D and 3D operation would mean the same thing or if they would have difference on the output. For some methods, for example the CLAHE filter, the MATLAB built in version did not have any support for three dimensional operations of the kind even though it would be mathematically possible. For many cases it is just computationally less heavy to work in 2D, so to try and keep the processing time down during the segmentation they did replace their 3D equivalents in some cases.

5.5 Animal model and ethical aspects

The data used in this thesis were the product of two experiments. These experiments have and are also being used in other research relating to this thesis. Testing was ethically approved by a regional ethics committee which means the experiment was designed to limit animal suffering in relation to the three R's of ethical animal use, replacement, reduction and refinement. Replacement means that animal testing should try to

be avoided or replaced by other possible methods if it is reasonable. The animal data was in these cases needed since there are no other methods to examine the development of mineral in relation to different loading or microinjuries. Reduction sees that the number of test animals are reduced in this testing but also in a bigger picture. Usually multiple test can be performed on the same animals to obtain more data, i.e. multiple planned tests might be performed by one group of animals. An evaluation of how many are necessary for the test should also be performed beforehand. For a newer study like this few animals can be used to identify if it is something to investigate further. The last R, refinement, refers to increasing the welfare and well-being of the animals. The key is to minimize the pain, suffering and distress of the animals subjected to the experiment.

Theoretically the fully loaded group from the first experiment and the control group from the needled data sets have the exact same loading scenario therefore they can be considered to be the same. Though combining these sets are possible, it would not be common practice. These animals have gone through the experiments at different moments in time which means there is no way to control that the conditions were the exact same. Limitations also occur when looking at the other groups, these are completely different and can not be combined in a meaningful way.

To be able to do a statistical data analysis more data is needed. For the needled sets there is only three samples for each group which means an average and a standard deviation do not provide statistically reliable information in regards of general behaviour of tendons with microdamage, though if there were substantial differences in behavior even a small number of samples would show it. All of our samples could for example without knowledge of it be uncommonly low or high. To get more confident results what needs to be done is probably more animal testing. Although since we can see a difference in between the groups in some regards, maybe the existing data is enough. Not conducting more experiments would be the more ethical choice.

5.6 Other possible approaches

This section contains a discussion of alternative solutions for the overarching methodology, for example using machine learning to segment or computer vision for stitching the sets. As for using machine learning instead of the methods describe in this report there are two different approaches, individual slice segmentation or total 3D volume segmentation. For individual slice segmentation the data provided by these data sets are probably enough size wise to both train and test on. Problems with this is partly that individual segmentation is not really what is of interested in, as mentioned before, consecutive slices can look very different in the segmentation although they should look almost the same. Possibly the machine could have some function that connects the new slice to the previous one but this would be a type of 3D segmentation. A 3D machine learning segmentation has one big shortcoming and that is the limited amount of data. It would not really be ethically defensible to produce more data for the sole use of machine learning. The upside of both methods is obviously maybe a better result could be produced and also it is more effective for the engineer to not have to trial different morphological changes and different thresholds.

To use computer vision as an alternative to the Big Stitcher could be an interesting new solution to sets that did not stitch. A discipline in computer vision is using landmarks of different images (either manually or somehow automatically placed) to see how they relate to each other. It is mostly done for 2D images to reconstruct the 3D environment it was taken in. Additional information except for the landmarks would need to be provided. An essential part is for example the camera location in relation to the sample, or not the necessarily camera location but the changes in camera location between images. This can probably be calculated using geometry.

5.7 Future perspective

It could also be interesting to examine the growth pattern of the minerals. This would require more animal testing where animals have their tendons harvested at different time points after testing. Since there are a wide array of mineral shapes throughout these sets there is no clear way to know if a tendon harvested after four weeks of testing will be fur-

ther along in heterotopic ossification formation than a tendon at three weeks because they would be from different test animals. To conduct a meaningful test of this kind another imaging method would need to be used so that the same animals can imaged in vivo at multiple time points.

Chapter 6

Conclusions

High resolution image data of the rat Achilles tendon was taken and segmentational methods for extracting the tendon and the mineral from the background was made. The segmentation was done in multiple programs and using different mathematical and image analysis techniques. Some processes did not work for all the samples which entailed creations of alternative solutions. These segmentations were analysed and data points relating to the volume and placement were extracted and compared.

The tendon and the mineral were successfully segmented from their surroundings. From these segmentations the data extracted showed only minor differences between the groups tested. Due to the small number of specimens in some testing groups statistically significant results were not possible to obtain. The data obtained from these segmentations can still be indicative that heterotopic ossifications occur due to different loading or needling scenarios. The group needled 20 times was the most different when observing the size of the mineralization which indicated some effect was seen from the needling.

This thesis work has prepared some ground for continuing to work on understanding the heterotopic ossifications of the tendon. Other ways to analyse the data can be developed from the segmentations but also by analysing the raw data in new ways. The methods developed could also be modified and used for segmentations from similar image data depicting other tissues such as cartilage and ligaments.

Bibliography

[1] James H.-C. Wang. Mechanobiology of tendon. *Journal of Biomechanics*, 39(9):1563–1582, 2006.

[2] M. Hammerman, F. Dietrich-Zagonel, P. Blomgran, P. Eliasson, and P. Aspenberg. Different mechanisms activated by mild versus strong loading in rat achilles tendon. *PLOS ONE*, 13, 2018.

[3] Lin Xuemei, Huang Minjun, Yin Ganghui, Zhang Jie, Zhang Zhongmin, Lai Pinglin, Yan Bo, Chen Yuhui, Jin Dadi, and Wang Liang. Characterization of a novel calcific achilles tendinopathy model in mice: Contralateral tendinopathy induced by unilateral tenotomy. *Calcified tissue international*, 103(6):698—707, December 2018.

[4] Carolyn Ann Meyers, Jeffrey L. Lisiecki, Sarah Miller, Adam S. Levin, Laura Marie Fayad, Catherine Ding, Takashi Sono, Edward F. McCarthy, Benjamin Levi, and Aaron Watkins James. Heterotopic ossification: A comprehensive review. *JBMR Plus*, 3, 2019.

[5] M. Saccomano, J. Albers, G. Tromba, Marina Dobrivojević Radmilović, S. Gajović, F. Alves, and C. Dullin. Synchrotron inline phase contrast ct enables detailed virtual histology of embedded soft-tissue samples with and without staining. *Journal of synchrotron radiation*, 25 Pt 4:1153–1161, 2018.

[6] Maria Pierantoni, Isabella Silva Barreto, Malin Hammerman, Lissa Verhoeven, Elin Törnquist, Vladimir Novak, Rajmund Mokso, Pernilla Eliasson, and Hanna Isaksson. A quality optimization approach to image Achilles tendon microstructure by phase-contrast enhanced synchrotron micro-tomography. *Scientific Reports*, 11(1):17313, 2021.

[7] Doral MN, Alam M, Bozkurt M, Turhan E, Atay OA, Dönmez G, and Maffulli N. Functional anatomy of the achilles tendon. *Knee Surg Sports Traumatol Arthrosc*, (18):638–643, May 2010.

[8] Franchi M, Trirè A, Quaranta M, Orsini E, and Ottani V. Collagen structure of tendon relates to function. *ScientificWorldJournal*, 7:404–420, March 2007.

[9] Alan M. Wilson and G. Lichtwark. The anatomical arrangement of muscle and tendon enhances limb versatility and locomotor performance. *Philosophical Transactions of the Royal Society B: Biological Sciences*, 366:1540 – 1553, 2011.

[10] Andrea H. Lee and Dawn M. Elliott. Comparative multi-scale hierarchical structure of the tail, plantaris, and achilles tendons in the rat. *Journal of Anatomy*, 234(2):252–262, 2019.

[11] Frederick H. Silver, Joseph W. Freeman, and Gurinder P. Seehra. Collagen self-assembly and the development of tendon mechanical properties. *Journal of Biomechanics*, 36(10):1529–1553, 2003. Bone Cell and Tissue Mechanics.

[12] Masaki Yanagishita. Function of proteoglycans in the extracellular matrix. *Pathology International*, 43(6):283–293, 1993.

[13] Laboratories Servier. Tendon anatomy tendon epimysium fascicle fiber fibril. `https://commons.wikimedia.org/wiki/File:Tendon_anatomy_-_Tendon_Epimysium_Fascicle_Fiber_Fibril_etc_--_Smart-Servier_(cropped).jpg`. Accessed: 2020-10-24, Published: 2019-09-29.

[14] Robert F. Ker. Mechanics of tendon, from an engineering perspective. *International Journal of Fatigue*, 29(6):1001–1009, 2007.

[15] Geoffrey Handsfield, Laura Slane, and Hazel Screen. Nomenclature of the tendon hierarchy: An overview of inconsistent terminology and a proposed size-based naming scheme with terminology for multi-muscle tendons. *Journal of Biomechanics*, 49, 06 2016.

[16] Mark L. Wood, Gayle E. Lester, and Laurence E. Dahners. Collagen fiber sliding during ligament growth and contracture. *Journal of Orthopaedic Research*, 16(4):438–440, 1998.

[17] Adam Zysk, Alfred Garson, Qiaofeng Xu, Eric Brey, Wei Zhou, Jovan Brankov, Miles Wernick, Jerome Kuszak, and Mark Anastasio. Nondestructive volumetric imaging of tissue microstructure with benchtop x-ray phase-contrast tomography and critical point drying. *Biomedical optics express*, 3:1924–32, 08 2012.

[18] Susha Cheriyedath. Micro-ct principles, strengths, and weaknesses, Feb 2019. Acessed: Oct 6 2021.

[19] Shu-Ang Zhou and Anders Brahme. Development of phase-contrast x-ray imaging techniques and potential medical applications. *Physica Medica*, 24(3):129–148, Sep 2008.

[20] Núñez Juan A et al. Simultaneous visualisation of calcified bone microstructure and intracortical vasculature using synchrotron x-ray phase contrast-enhanced tomography. *Scientific reports*, 7, October 2017.

[21] Preibisch Stephan, Saalfeld Stephan, and Tomancak Pavel. Globally optimal stitching of tiled 3D microscopic image acquisitions. *Bioinformatics*, 25(11):1463–1465, 04 2009.

[22] Nobuyuki Otsu. A threshold selection method from gray-level histograms. *IEEE Transactions on Systems, Man, and Cybernetics*, 9(1):62–66, 1979.

[23] 31 - video signal processing. In Charles Poynton, editor, *Digital Video and HD (Second Edition)*, The Morgan Kaufmann Series in Computer Graphics, pages 377–388. Morgan Kaufmann, Boston, second edition edition, 2012.

[24] İmren Dinç, Semih Dinç, Madhav Sigdel, Madhu S. Sigdel, Ramazan S. Aygün, and Marc L. Pusey. Chapter 12 - dt-binarize: A decision tree based binarization for protein crystal images. In Leonidas Deligiannidis and Hamid R. Arabnia, editors, *Emerging Trends in Image Processing, Computer Vision and Pattern Recognition*, pages 183–199. Morgan Kaufmann, Boston, 2015.

[25] Etta D. Pisano, Shuquan Zong, Bradley M. Hemminger, Marla DeLuca, R. Eugene Johnston, Keith E. Muller, M. Patricia Braeuning, and Stephen M. Pizer. Contrast limited adaptive histogram equalization image processing to improve the detection of simulated

spiculations in dense mammograms. *J. Digit. Imaging*, 11(4):193–200, 1998.

[26] Justin Joseph, J. Sivaraman, R. Periyasamy, and V.R. Simi. An objective method to identify optimum clip-limit and histogram specification of contrast limited adaptive histogram equalization for mr images. *Biocybernetics and Biomedical Engineering*, 37(3):489–497, 2017.

[27] Renato Keshet. Erosion. `https://commons.wikimedia.org/wiki/File:Erosion.png`. Accessed: 2020-10-24, Published: 2008-07-06.

[28] Renato Keshet. Dilation. `https://commons.wikimedia.org/wiki/File:Dilation.png`. Accessed: 2020-10-24, Published: 2008-07-07.

[29] Renato Keshet. Closing. `https://commons.wikimedia.org/wiki/File:Closing.png`, note = Accessed: 2020-10-24, Published: 2008-07-09.

[30] Renato Keshet. Opening. `https://commons.wikimedia.org/wiki/File:Opening.png`. Accessed: 2020-10-24, Published: 2008-07-07.

[31] Hanifeh Khayyeri, Parmis Blomgran, Malin Hammerman, Mikael J. Turunen, Annika Löwgren, Manuel Guizar-Sicairos, Per Aspenberg, and Hanna Isaksson. Achilles tendon compositional and structural properties are altered after unloading by botox. *Scientific Reports*, 7(1), December 2017.